

A Comprehensive Study of Decoder-Only LLMs for Text-to-Image Generation

Andrew Z. Wang^{1,3†} Songwei Ge^{2†} Tero Karras³ Ming-Yu Liu³ Yogesh Balaji³
¹University of Washington ²University of Maryland ³NVIDIA

Abstract

Both text-to-image generation and large language models (LLMs) have made significant advancements. However, many text-to-image models still employ the somewhat outdated T5 and CLIP as their text encoders. In this work, we investigate the effectiveness of using modern decoder-only LLMs as text encoders for text-to-image diffusion models. We build a standardized training and evaluation pipeline that allows us to isolate and evaluate the effect of different text embeddings. We train a total of 27 text-to-image models with 12 different text encoders to analyze the critical aspects of LLMs that could impact text-to-image generation, including the approaches to extract embeddings, different LLMs variants, and model sizes. Our experiments reveal that the *de facto* way of using last-layer embeddings as conditioning leads to inferior performance. Instead, we explore embeddings from various layers and find that using layer-normalized averaging across all layers significantly improves alignment with complex prompts. Most LLMs with this conditioning outperform the baseline T5 model, showing enhanced performance in advanced visio-linguistic reasoning skills.

1. Introduction

The field of text-to-image generation has seen tremendous progress in recent years, driven by improvements in diffusion architectures [6, 12, 35], scalable models [41, 42], and better training procedures [27, 28, 35]. Central to the success of these models is the use of pre-trained text encoders that transfer natural language prompts into representations suitable for guiding image generation. However, the impact of different text encoder models on the image generation quality remains largely unexplored.

Most contemporary image generators use traditional text encoders such as T5 [44] or CLIP [43] for obtaining text embeddings [1, 2, 42, 45, 48]. However, the development of encoder-decoder models has slowed down while there is an increasing interest in decoder-only large language models (LLMs) due to their great scalability. This raises a pressing

[†]This work was done during an internship at NVIDIA.

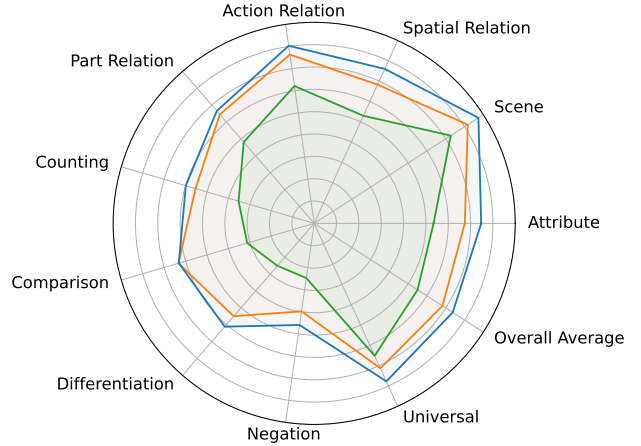


Figure 1. VQA scores for text-to-image models using T5-XXL and Mistral-7B as the text encoders. The models use embeddings extracted from the last layer of T5 (orange) and Mistral (green), and layer-normalized average embeddings of Mistral (blue). Our results show that Mistral performs worse than T5 when only using the last layer. However, using all layers significantly improves Mistral’s performance, surpassing T5 in all aspects.

question of whether these decoder-only LLMs are suitable for text-to-image generation tasks.

In this work, we examine how the rich linguistic representations from decoder-only LLMs can be leveraged to enhance text-to-image generation and investigate the most effective strategies for incorporating them. Our focus is on autoregressive language models that use causal attention and are trained with a next-token prediction objective. We address three primary research questions:

1. To what extent can decoder-only LLMs be utilized to enhance text-to-image generation? What methodologies yield the largest improvements?
2. LLM fine-tuned embedding models have surpassed encoder-decoder models in contextual semantic comprehension across various tasks [40]. Can these embedding models contribute to improving text-to-image alignment?
3. Does increasing the model size of decoder-only LLMs

lead to measurable improvements in the text-to-image generation performance?

To address these questions, we develop a standardized text-to-image training and evaluation pipeline based on the Stable Diffusion v2 (SD2) [46] architecture. In each experiment, only the text encoder is replaced, while the rest of the architecture and training recipe remains unchanged. This allows us to isolate and understand the effect of different text representations. We explore a wide variety of models as text encoders, including two traditional text-to-image text encoders, seven open-source LLMs, and three fine-tuned embedding models. We quantitatively evaluate the models using VQAScore [30] on GenAI-Bench [30], and conduct in-depth analysis to understand the strengths and limitations of using LLMs as the text encoders. Our main findings are as follows:

- **Using text embeddings from the last layer of the LLM is sub-optimal:** To our knowledge, all current text-to-image diffusion models utilize the embeddings from the final layer of the text encoders as the conditional embedding [2, 48]. However, our results reveal that this approach does not translate effectively to LLMs, leading to inferior results compared to using T5.
- **Aggregating features from multiple layers outperforms using a single layer:** We find that using embeddings normalized and averaged across all layers yields far better performance than relying on any single layer alone (Figure 1). This is because each layer within an LLM captures different aspects of linguistic information, so using averaged embeddings can combine the strengths of every layer to create a richer and more comprehensive representation [11, 24, 37].
- **LLM-based embedding models sometimes outperform the base models:** Our results suggest that fine-tuned embedding models hold the potential for improving text-to-image generation. However, such a performance improvement is not always observed across all the embedding and base models. Despite these mixed outcomes, strong results are achieved with bge-Gemma2 [8] using layer-normalized average embeddings, our best-performing model, highlighting promise in leveraging embedding models for text-to-image generation.
- **Scaling up the LLM is beneficial, but not across all aspects:** Increasing the model size of LLMs consistently leads to improved performance. However, we observe that model size does not uniformly enhance all aspects of compositional text-to-image generation. These results suggest that simply scaling model size may not be the most efficient approach for improving performance across all skills, highlighting the potential of alternative strategies, such as hybrid models or skill-specific fine-

tuning.

2. Related work

Text encoders in text-to-image generation. In recent years, a variety of text encoders have been explored for training large-scale diffusion models. DALLE2 [45] and Stable Diffusion [46] use text embeddings from the CLIP [43] model that is trained using an image-text alignment objective. Imagen [48] showed that the embeddings from pure language models such as T5 [44] can be used for image generation and that scaling the language models can improve the image generation performance. eDiff-I [2] observed that the use of CLIP and T5 can give complementary benefits and propose the use of a combination of both these embeddings. Liu et al. [36] showed that using character-aware tokenizers like ByT5 [62] can improve text rendering while generating images.

Decoder-only LLMs. Several studies have looked into exploiting LLMs for text-to-image generation. Earlier works utilized LLMs as inputs through adapter connectors [16, 20] and explored their sequence-to-sequence capabilities to revise prompts [7] or build scene layouts [32]. The recent concurrent work of Playground-v3 [35] conditions different blocks of the diffusion transformer model using embeddings from intermediate layers of a Llama3 [15] model. Lumina-T2X [13] uses the output layer of a LLama-7B [56] model as the text encoder, while Lumina-Next [67] and Sana [61] use the embeddings from Gemma-2-2B [52] model.

LLM interpretability. As we are interested in analyzing the best ways to utilize LLMs, a relevant line of research is on analyzing the linguistic representations captured across different layers within LLMs [11, 24, 37, 54, 65]. Some studies have addressed the contextual limitations imposed by causal attention masks in autoregressive models [50], while others have examined approaches to best extract embedding representations from LLMs [4, 8, 26, 31, 58, 59].

While these recent works investigate the use of various text encoders for image generation, their models are trained on different datasets (often proprietary) and with varying training setups, making it difficult to isolate the role of text encoders. The goal of this work is to perform a systematic study on the effect of different text encoders, aiming to deepen understanding of how text representations influence text-image alignment and generation quality.

3. Experimental setup

3.1. Training pipeline

To understand the impact of text encoders in text-to-image diffusion models, we first establish a standard model train-



Figure 2. Visual comparison of images generated with different text encoders. We use last-layer embeddings (*last layer*) from the text encoders of [CLIP-ViT-H/14](#) (354M) and [T5-XXL](#) (4.7B). We also use average layer-normalized embeddings (*norm avg*) from the pre-trained LLM [Mistral-7B](#) (7B) and the fine-tuned embedding model [bge-Gemma2](#) ([bge-multilingual-gemma2](#); 9B). Mistral and bge-Gemma2 can handle complex reasoning tasks such as negation (panel below) compared to models like CLIP and T5.

ing pipeline, enabling us to isolate the effect of text encoders from other factors, like diffusion model architecture, training data, and compute. For all our experiments, we utilize the U-Net based latent diffusion architecture from Stable Diffusion [46]. We freeze the autoencoder and only train the U-Net model [47], in which text embeddings are conditioned using cross attention blocks. To accommodate the different text embedding dimension sizes from various models, we introduce a linear projection layer with 1024 output features before cross-attention in the U-Net. In each experiment, we replace the text encoder with a different LLM or fine-tuned embedding model. The exact training recipe, including batch size, diffusion process, and other hyperparameters are also adapted from Stable Diffusion [46]. Please find more details in the supplementary material.

We utilize a 46 million text-image pair subset of the LAION-Aesthetics dataset [49] as the training data. For enhanced caption diversity and richness, we apply VisualFactChecker (VFC) [14], an LLM-based technique for

performing caption upsampling. We train all models for 800,000 iterations at 256×256 resolution with a global batch size of 2,048 on 32 A100 GPUs. Each model has around 870M parameters and takes approximately 7 days to train.

3.2. Models of interest

We mainly explore four types of text encoders:

- T5: [T5-XXL](#) (encoder size ≈ 4.7 B params) [44] is an encoder-decoder model that frames NLP tasks in a unified text-to-text format, utilizing a span-masked language model objective. Its text encoder is widely used in text-to-image models to effectively capture linguistic and semantic information for image generation.
- CLIP: [CLIP-ViT-H/14](#) (encoder size ≈ 354 M params) [43] aligns visual and textual representations within a shared embedding space through contrastive learning, making it a popular choice for text-to-image generation

Model	Size	Avg	Attr.	Scene	Spat.	Action	Part	Count.	Comp.	Differ.	Neg.	Uni.
CLIP _{ViT-H/14}	354M	0.622	0.612	0.731	0.608	0.655	0.594	0.529	0.522	0.425	0.480	0.632
T5-XXL	4.7B	0.741	0.737	0.809	0.741	0.782	0.723	0.677	0.717	0.675	0.599	0.757
Qwen2-7B	7B	0.683	0.679	0.805	0.670	0.724	0.657	0.588	0.603	0.590	0.552	0.763
Mistral-7B	7B	0.675	0.667	0.763	0.665	0.711	0.641	0.576	0.556	0.526	0.524	0.726
Llama3-8B	8B	0.675	0.673	0.767	0.656	0.704	0.667	0.627	0.615	0.568	0.542	0.768
Gemma2-9B	9B	0.710	0.709	0.794	0.711	0.760	0.705	0.642	0.659	0.617	0.544	0.709
gte-Qwen2	7B	0.482	0.486	0.537	0.479	0.497	0.466	0.446	0.393	0.405	0.424	0.437
sfr-Mistral	7B	0.710	0.706	0.804	0.707	0.740	0.691	0.661	0.670	0.615	0.608	0.766
Mistral-7B _{Instruct}	7B	0.690	0.683	0.787	0.686	0.718	0.654	0.628	0.630	0.589	0.577	0.762
bge-Gemma2	9B	0.737	0.730	0.824	0.729	0.793	0.722	0.662	0.654	0.641	0.623	0.797

Table 1. VQAScore for models using embeddings extracted from the last layer. We use text encoders from CLIP-ViT-H/14 (354M) and T5-XXL (4.7B), along with four popular open-source pre-trained LLMs: Qwen2 (7B), Mistral-7B (7B), Llama3 (8B), and Gemma2 (9B). Additionally, we include three embedding models fine-tuned on these LLMs: gte-Qwen2 (gte-Qwen2-7B-instruct; 7B), sfr-Mistral (SFR-Embedding-2_R; 7B), and bge-Gemma2 (bge-multilingual-gemma2; 9B). We also include an instruction fine-tuned model, Mistral-7B-Instruct (7B). The highest scores are shown in **bold**. Our results show that only using the last layer does not work well for LLMs and perform worse than T5.

for strong text-image alignment.

- Pre-trained LLMs: **Mistral-7B** (and instruction fine-tuned **Mistral-7B-Instruct**) [25], **Gemma2** (2B and 9B) [52], **Llama3-8B** [15], **Qwen2** (1.5B and 7B) [63]. We include several open-source, high-performing LLMs in our study, each trained for autoregressive language modeling with a next token prediction objective. Although these models are all decoder-only transformers, they vary in terms of tokenization and other architectural details.
- LLM fine-tuned embedding models: **bge-Gemma2** (bge-multilingual-gemma2; 9B) [8], **gte-Qwen2** (gte-Qwen2-7B-instruct; 7B) [31], **sfr-Mistral** (SFR-Embedding-2_R; 7B) [39]. We also evaluate fine-tuned versions of the LLMs mentioned above, specifically selected from top performing models on the Massive Text Embedding Benchmark (MTEB) Leaderboard¹ [40]. We aim to examine whether improvements in semantic comprehension translate into improved image generation and text-image alignment.

3.3. Benchmarking and metrics

To evaluate and compare the performance of different models, we adopt GenAI-Bench [34] as our primary benchmarking suite. GenAI-Bench includes 1,600 diverse and challenging prompts, and each prompt is annotated with specific aspects in the compositional text-to-visual generation: *Attribute*, *Scene*, *Spatial Relation*, *Action Relation*, *Part Relation*, *Counting*, *Differentiation*, *Comparison*, *Negation*, and *Universality* [30, 34]. These skill annotations enable us

¹ All ranked top 10 on the MTEB Leaderboard as of Nov. 2024.

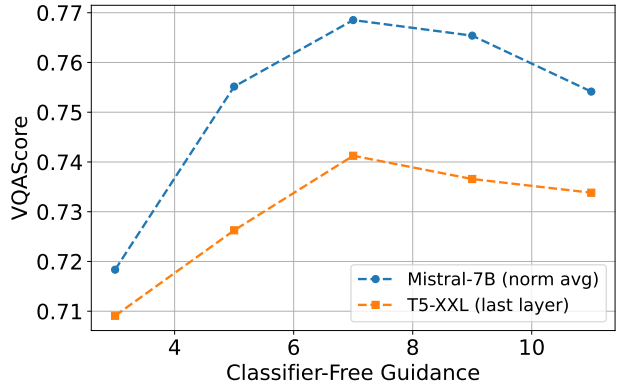


Figure 3. VQAScore as a function of classifier-free guidance weight. We show the VQAScore of Mistral-7B using layer-normalized average embeddings (blue) and T5-XXL using last-layer embeddings (orange) at varying guidance strengths.

to conduct in-depth ablation studies, allowing for detailed analysis of how various LLMs and embedding extraction methods affect specific aspects of text-to-image generation. To better align the prompts with our upsampled training distribution, we utilize Gemma2-9B [52] for prompt upsampling as detailed in the supplementary material.

Previous research has shown that traditional text-image evaluation metrics like CLIPScore [17] and FID [18] are not consistent with human evaluations, particularly in assessing complex compositional tasks [3, 30, 34]. Instead, VQA-based automatic evaluation methods have demonstrated higher reliability and correlation with human judgments [9, 21, 22, 30, 34, 60, 64]. Our observations are con-

Model	Layer	Avg	Attr.	Scene	Spat.	Action	Part	Count.	Comp.	Differ.	Neg.	Uni.
T5-XXL	25 (last)	0.741	0.737	0.809	0.741	0.782	0.723	0.677	0.717	0.675	0.599	0.757
Mistral-7B	33 (last)	0.675	0.667	0.763	0.665	0.711	0.641	0.576	0.556	0.526	0.524	0.726
Mistral-7B	32	0.710	0.718	0.794	0.707	0.747	0.686	0.638	0.625	0.650	0.582	0.703
Mistral-7B	15	0.725	0.720	0.812	0.729	0.762	0.692	0.673	0.651	0.647	0.585	0.732
Mistral-7B	0 (first)	0.375	0.372	0.499	0.339	0.379	0.290	0.297	0.328	0.200	0.278	0.440

Table 2. VQAScore for models using embeddings extracted from individual layers of **Mistral-7B** (7B). We include the baseline **T5-XXL** (4.7B) model using embeddings extracted from the last layer as a reference. The highest scores are shown in **bold**. Our results show that using middle layers can outperform earlier or later layers.

Model	Embeddings	Avg	Attr.	Scene	Spat.	Action	Part	Count.	Comp.	Differ.	Neg.	Uni.
T5-XXL	last layer	0.741	0.737	0.809	0.741	0.782	0.723	0.677	0.717	0.675	0.599	0.757
T5-XXL	norm avg	0.747	0.748	0.813	0.745	0.780	0.720	0.687	0.736	0.675	0.617	0.760
bge-Gemma2	last layer	0.737	0.730	0.824	0.729	0.793	0.722	0.662	0.654	0.641	0.623	0.797
bge-Gemma2	avg	0.774	0.776	0.851	0.765	0.813	0.752	0.716	0.773	0.702	0.665	0.822
bge-Gemma2	norm avg	0.789	0.787	0.846	0.782	0.821	0.786	0.745	0.776	0.744	0.712	0.810
Mistral-7B	last layer	0.675	0.667	0.763	0.665	0.711	0.641	0.576	0.556	0.526	0.524	0.726
Mistral-7B	avg	0.731	0.733	0.806	0.731	0.779	0.712	0.683	0.666	0.639	0.582	0.758
Mistral-7B	norm avg	0.769	0.774	0.837	0.780	0.802	0.733	0.699	0.716	0.706	0.630	0.789

Table 3. VQAScore for models using different embedding strategies: standard last-layer embeddings (*last layer*), average embeddings across all layers (*avg*), and average embeddings across all normalized layers (*norm avg*). We apply these approaches to the encoder from the baseline **T5-XXL** (4.7B), the pre-trained LLM **Mistral-7B** (7B), and our best performing fine-tuned embedding model **bge-Gemma2** (**bge-multilingual-gemma2**; 9B). The highest scores are shown in **bold**. Our results show that using layer-normalized averaging greatly enhances performance and outperforms T5.

sistent with these findings, so we use VQAScore [34] as our primary evaluation metric in this work. Notably, we also observe that the custom CLIP-FlanT5 [34] model that was originally proposed for VQAScore is not sufficient to differentiate between similar models [3]. To address this, we utilize GPT-4o [23] for our implementation of VQAScore, achieving improved differentiation between models and a closer match to human-perceived quality. When computing VQAScore, we generate the 1,600 images using the same seeds for each model. The random variation of VQAScore with GPT-4o is up to ± 0.003 , depending on the category. Please find more details in the supplementary material.

3.4. Classifier-free guidance

In our work, we use a classifier-free guidance [19] of 7.0 for all models. Figure 3 shows a line graph with VQAScore as a function of guidance weight. These results illustrate how different guidance strength affects VQAScore considerably, potentially even more than the choice of the text encoder. As such, we standardize guidance at 7.0 in our evaluation pipeline for apples-to-apples comparison. Similar to the original Stable Diffusion model [46], we do not employ any kind of thresholding [48] or rescaling [33].

4. Results

4.1. Final layer LLM embeddings lack in visio-linguistic reasoning

We begin by training text-to-image models using text encoders described in Sec. 3.2, extracting embeddings from the final layer, as commonly done in the literature [13, 48, 61, 67]. As shown in Table 1, replacing T5 with other LLMs consistently results in a decrease in performance. Most of the performance gap can be attributed to the advanced visio-linguistic reasoning skills in GenAI-Bench: *Counting*, *Differentiation*, *Comparison*, *Negation*, and *Universality*. Specifically, *Comparison* shows the most significant drop in performance relative to T5. In fact, when prompts tagged with *Comparison* are excluded, the results for the LLMs are similar to or even better than T5.

On the other hand, CLIP demonstrates one of the lowest scores overall, likely due to a combination of its much smaller model size, shorter token sequence length of 77, and reduced ability to capture linguistic and semantic details compared to the other language models [5, 43, 55]. For these reasons, we use T5 as the primary baseline in subsequent analysis.

Model	Avg	Attr.	Scene	Spat.	Action	Part	Count.	Comp.	Differ.	Neg.	Uni.
bge-Gemma2	0.737	0.730	0.824	0.729	0.793	0.722	0.662	0.654	0.641	0.623	0.797
bge-Gemma2 _{pooled}	0.737	0.733	0.838	0.725	0.767	0.712	0.692	0.691	0.663	0.641	0.823
sfr-Mistral	0.710	0.706	0.804	0.707	0.740	0.691	0.661	0.670	0.615	0.608	0.766
sfr-Mistral _{pooled}	0.698	0.685	0.810	0.693	0.748	0.694	0.610	0.641	0.596	0.589	0.730

Table 4. VQAScore for models using embeddings extracted from the last layer compared to models with additional conditioning on global pooled embeddings [42]. We evaluate the fine-tuned embedding models bge (bge-multilingual-gemma2; 9B) and sfr (SFR-Embedding-2_R; 7B). We observe limited differences with the latter approach for embedding models.

Model	Size	Avg	Attr.	Scene	Spat.	Action	Part	Count.	Comp.	Differ.	Neg.	Uni.
Qwen2	1.5B	0.655	0.654	0.758	0.642	0.681	0.624	0.575	0.553	0.528	0.553	0.676
Qwen2	7B	0.683	0.679	0.805	0.670	0.724	0.657	0.588	0.603	0.590	0.552	0.763
Gemma2	2B	0.640	0.650	0.745	0.627	0.687	0.606	0.580	0.597	0.527	0.442	0.707
Gemma2	9B	0.710	0.709	0.794	0.711	0.760	0.705	0.642	0.659	0.617	0.544	0.709

Table 5. VQAScore for models with different LLM sizes, using embeddings extracted from the last layer. We evaluate the pre-trained LLMs: Qwen2 (1.5B), Qwen2 (7B), Gemma2 (2B), Gemma2 (9B). Our results show that LLM scaling improves performance but does not uniformly impact all aspects of image composition.

4.2. Embedding performance differs by layer

In addition to using the final layer, we experiment with embeddings extracted from other individual layers within the Mistral-7B model to assess how semantic and linguistic representations across layers vary and impact image generation. The Mistral model, with its 33 layers, has been the focus of several works exploring embedding representations² [4, 25, 50, 59]. Table 2 shows that using only the 15th layer of Mistral outperforms the use of the 33rd (last), 0th (first), and 32nd (penultimate) layers. This suggests that different layers of LLMs capture distinct levels of semantic and linguistic understanding [11]. Early layers may primarily encode basic linguistic structures, while later layers tend to be specialized in next-token prediction [37]. By contrast, middle layers appear to offer a more balanced abstraction of semantic representations, which can better support image generation tasks. However, the baseline last layer T5 model still outperforms any single layer Mistral model. This leads to a key insight: **using embeddings from any single layer of the LLMs for text-to-image models is not sufficient.**

4.3. Averaging layers yields stronger embeddings

Since different layers in LLMs encode varying levels of semantic representations, we propose to aggregate the embeddings using two approaches. The first method involves directly averaging the embeddings across all layers. In the second approach, we apply mean normalization to each layer’s embeddings before averaging. This ensures that

each layer contributes consistently in scale, preventing any single layer from disproportionately influencing the aggregated representation [65]. We apply these approaches to Mistral and bge-Gemma2, our best performing embedding model. We show our results in Table 3 and Figure 1. More results with other models, such as Qwen2 and Llama3, can be found in supplementary material Table B. For both models, averaged embeddings yield substantial improvements over using only the last layer, even surpassing the baseline T5 model by a large margin. Notably, these approaches overcome the previously observed limitations in advanced visio-linguistic reasoning, demonstrating that embeddings derived from all layers produce richer and more comprehensive representations.

Our experiments also reveal that applying layer normalization beforehand performs even better than only averaging, as it balances contributions from each layer and prevents any single layer from dominating the representation. This leads to another key finding: **the most effective way to utilize LLMs for text-to-image models is to properly use embeddings from all layers.**

Interestingly, applying layer-normalized averaging to T5 embeddings shows almost no performance difference. We believe this is due to the T5 encoder’s approach of framing each task in a text-to-text format, and its later layers inherently build upon the semantic and linguistic foundations established in earlier layers. In contrast, the later layers of decoder-only LLMs tend to specialize in next-token prediction, which explains the significant performance gains observed when utilizing embeddings from intermediate layers.

²Llama3, another popular LLM, has [untrained token embedding issues](#)

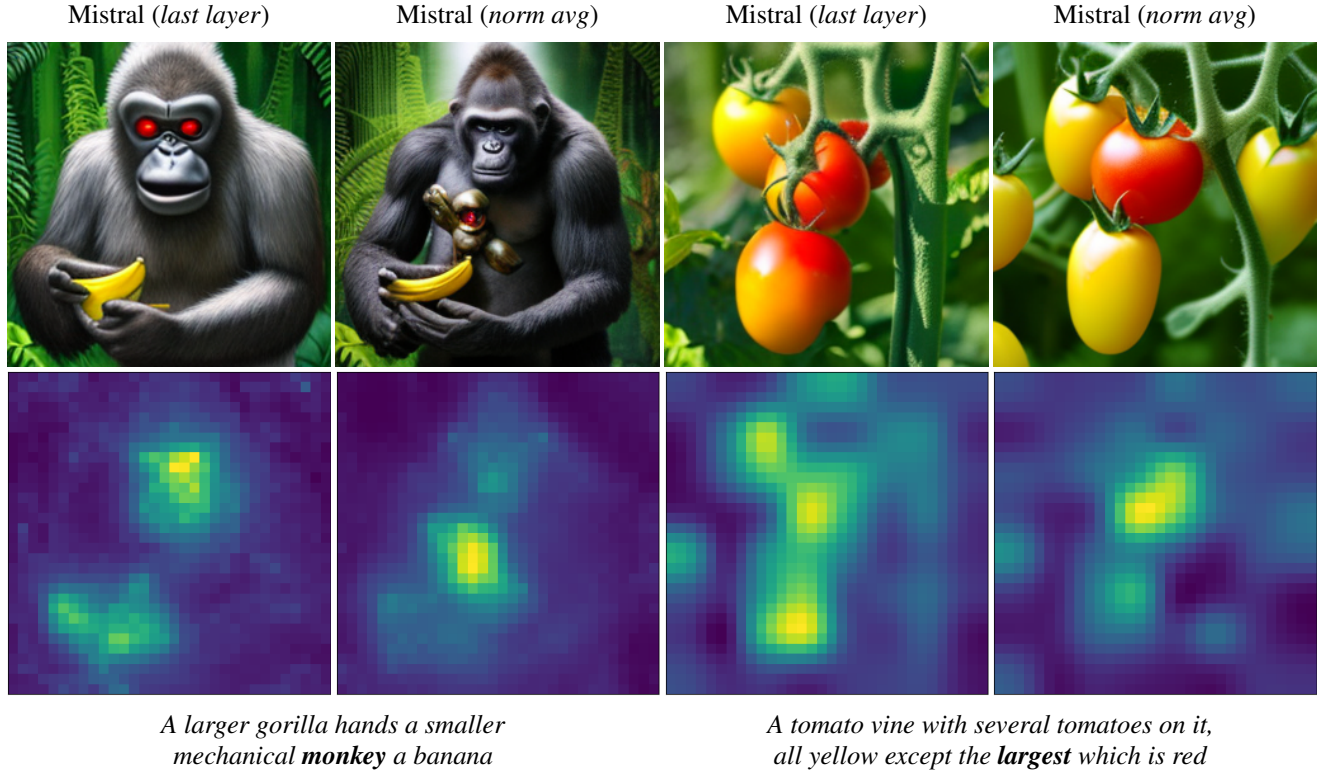


Figure 4. Heatmap visualization. Images generated with Mistral-7B using standard last-layer embeddings (*last layer*) and layer-normalized average embeddings (*norm avg*). Corresponding cross-attention heatmaps for the tokens **monkey** (left set) and **largest** (right set) are shown in the panel below. These visualizations show how the *norm avg* model performs better than *last layer* model on prompts that require advanced visio-linguistic reasoning skills such as *differentiation* (left set) and *comparison* (right set).

4.4. Finetuned embedding models show potential

Our results in Table 1 indicate that fine-tuned embedding models can offer improvement over their pre-trained LLM counterparts, as seen with bge-Gemma2 and sfr-Mistral, but may also lead to significant performance degradation, as with gte-Qwen2. We suspect this inconsistency arises because most fine-tuned embedding models are optimized to produce pooled embeddings primarily through methods like last token pooling, mean pooling, or weighted mean pooling. These pooling strategies may impact the embeddings of individual tokens, resulting in less meaningful representations across the entire sequence [29, 50].

We also experiment with a SDXL [42] inspired approach by conditioning the text-to-image models on two types of embeddings: standard per-token embeddings and a single pooled text embedding as a condensed global representation. Individual tokens go to cross-attention, while the pooled token is combined with the timestep embedding to modulate layer activations. Since these embedding models are primarily designed to produce a single pooled embedding, this approach enables us to incorporate their intended use case fully for better comparison to our baseline models.

We selected bge-Gemma2 and sfr-Mistral for their improvement over their base models. However, as shown in Table 4, we observe limited differences in performance with this method, suggesting that our approach may not fully leverage the potential of these embeddings.

Despite these mixed results, **there is considerable promise in using embedding models for text-to-image generation**, as demonstrated by the bge-Gemma2 model with layer-normalized averaging, which is the best performing model in our experiments. Future research to determine the most effective strategies could explore hybrid pooling approaches that combine per-token embeddings from pre-trained LLMs with additional conditioning from pooled embeddings in fine-tuned embedding models. Adding an extra latent attention layer, proposed by NV-Embed [29], could also improve the quality of pooled embeddings.

4.5. Scaling improves performance, but not uniformly across compositional skills

Prior research has shown that scaling the size of the text encoder yields greater improvements in image quality and text-image alignment compared to increasing the size of the diffusion model [48]. In our experiments, we evalu-

ate different LLM model sizes to understand the impact of scaling on performance. Our results on differently sized Qwen2 and Gemma2 models in Table 5 confirm these findings. Although our ablation experiments are limited to a subset of models, the skill annotations from GenAI-Bench reveal an interesting insight: **while performance increases with model size, scaling does not uniformly impact all aspects of compositional text-to-visual generation**. For instance, we observe minimal improvement in *Negation* and *Counting* between the two Qwen2 models, while the difference in *Universality* is significant. Conversely, the two Gemma2 models show little difference in *Universality* but exhibit substantial differences across most other skills.

Given the minimal improvements in specific skills, these results raise questions about the efficiency of simply scaling model size for text-to-image generation. Future work could explore hybrid approaches, such as combining different LLMs to leverage complementary strengths. This is similar to how eDiff-I [2] combined the T5 and CLIP text encoders to enhance embedding representations. Smaller, specialized models fine-tuned on skill-specific tasks might also provide a more efficient way to improve performance.

Additionally, it would be valuable to investigate the effects of scaling text encoders when fully utilizing all layers, such as our approaches using layer-normalized averaging. This could reveal whether more refined approaches to layer utilization might achieve comparable or even superior results to model scaling.

5. Visual analysis

As shown in Sections 4.1 and 4.3, LLMs demonstrate significant improvements in advanced visio-linguistic reasoning when using layer-normalized average embeddings. Figure 2 provides a visual comparison with T5 and CLIP models for handling *negation*, where the baselines fail to interpret such logic and incorrectly depict the dog wearing clothes. Additional comparisons are available in the supplementary material. We observe these enhanced logical abilities in our models with Mistral through visual comparisons and cross-attention heatmaps on relevant tokens:

Differentiation. The left set of images in Figure 4 illustrate a *differentiation* prompt involving a gorilla and a mechanical monkey. The model using last-layer embeddings fails to distinguish between the two, rendering the gorilla with robotic features but omitting the monkey. Cross-attention heatmaps for the token *monkey* show that attention is focused on the gorilla, indicating a lack of differentiation.

In contrast, the model using averaged layer-normalized embeddings successfully separates the two entities. The cross-attention heatmap for *monkey* shows distinct attention away from the gorilla, allowing the mechanical monkey to appear separately. This suggests that layer-normalized averaging helps the model better differentiate semantically

similar objects, as seen in the increased embedding norm distinction between gorilla and monkey. Additionally, we observe that the difference in token embedding norms for *gorilla* and *monkey* is greater in layer-normalized averaging compared to the last layer. This increased distinction in embedding norms likely contributes to the model’s improved differentiation ability.

Comparison. The right set of images in Figure 4 show results for *comparison* prompts, where only the largest tomato should be red. With last-layer embeddings, multiple tomatoes appear red, indicating the model’s struggle to interpret logical constraints. Cross-attention heatmaps for *largest* show diffused attention, which contributes to misalignment with the prompt.

In contrast, layer-normalized average embeddings lead to better alignment with the prompt, focusing attention on the largest tomato and accurately rendering it as red while keeping the others yellow. However, neither model successfully represents the largest tomato as larger than the others, suggesting that further research is needed to explore how size-related cues are embedded and translated to image generation for improved spatial and comparative alignment.

6. Conclusion

Our research contributes to the evolving field of text-to-image generation by exploring the use of decoder-only LLMs as the text encoder. Through a controlled training pipeline, we isolate and evaluate the impact of different text encoders, conducting extensive experiments on various LLMs and embedding extraction methods.

Our findings provide valuable insights into using decoder-only LLMs for text-to-image generation. We demonstrate that relying on a single layer from an LLM is insufficient and propose a simple yet effective approach that leverages all layers through averaged layer-normalized embeddings. With this approach, our models exhibit significant improvements in advanced visio-linguistic reasoning skills, outperforming the baseline T5 model across all aspects of compositional text-to-image generation. Furthermore, our experiments with fine-tuned embedding models reveal promising potential for enhanced contextual semantic comprehension. Additionally, we explore the scalability of LLMs, observing that while performance generally increases with model size, specific compositional skills do not uniformly benefit from scaling.

This work opens several avenues for future research, including more refined approaches to layer aggregation, optimized usage of embedding models, and the development of hybrid models that combine multiple LLMs. By providing a detailed examination of decoder-only LLMs in text-to-image generation, we hope our insights will guide future advancements and extend to other multimodal applications.

References

- [1] Yuval Atzmon, Maciej Bala, Yogesh Balaji, Tiffany Cai, Yin Cui, Jiaojiao Fan, Yunhao Ge, Siddharth Gururani, Jacob Huffman, Ronald Isaac, et al. Edify image: High-quality image generation with pixel space laplacian diffusion models. *arXiv preprint arXiv:2411.07126*, 2024. 1
- [2] Yogesh Balaji, Seungjun Nah, Xun Huang, Arash Vahdat, Jiaming Song, Qinsheng Zhang, Karsten Kreis, Miika Aittala, Timo Aila, Samuli Laine, et al. ediff-i: Text-to-image diffusion models with an ensemble of expert denoisers. *arXiv preprint arXiv:2211.01324*, 2022. 1, 2, 8
- [3] Jason Baldridge, Jakob Bauer, Mukul Bhutani, Nicole Brichtova, Andrew Bunner, Lluís Castrejón, Kelvin Chan, Yichang Chen, Sander Dieleman, Yuqing Du, et al. Imagen 3. *arXiv preprint arXiv:2408.07009*, 2024. 4, 5
- [4] Parishad BehnamGhader, Vaibhav Adlakha, Marius Mosbach, Dzmitry Bahdanau, Nicolas Chapados, and Siva Reddy. Llm2vec: Large language models are secretly powerful text encoders. *arXiv preprint arXiv:2404.05961*, 2024. 2, 6
- [5] Santiago Castro, Oana Ignat, and Rada Mihalcea. Scalable performance analysis for vision-language models. *arXiv preprint arXiv:2305.18786*, 2023. 5
- [6] Junsong Chen, Jincheng Yu, Chongjian Ge, Lewei Yao, Enze Xie, Yue Wu, Zhongdao Wang, James Kwok, Ping Luo, Huchuan Lu, et al. PixArt-alpha: Fast Training of Diffusion Transformer for Photorealistic Text-to-Image Synthesis. *arXiv preprint arXiv:2310.00426*, 2023. 1
- [7] Jingye Chen, Yupan Huang, Tengchao Lv, Lei Cui, Qifeng Chen, and Furu Wei. Textdiffuser-2: Unleashing the power of language models for text rendering. In *ECCV*, 2024. 2
- [8] Jianlv Chen, Shitao Xiao, Peitian Zhang, Kun Luo, Defu Lian, and Zheng Liu. Bge m3-embedding: Multilingual, multi-functionality, multi-granularity text embeddings through self-knowledge distillation. *arXiv preprint arXiv:2402.03216*, 2024. 2, 4
- [9] Jaemin Cho, Abhay Zala, and Mohit Bansal. Visual programming for step-by-step text-to-image generation and evaluation. In *NeurIPS*, 2023. 4
- [10] Tri Dao, Dan Fu, Stefano Ermon, Atri Rudra, and Christopher Ré. Flashattention: Fast and memory-efficient exact attention with io-awareness. In *NeurIPS*, 2022. 1
- [11] Guy Dar, Mor Geva, Ankit Gupta, and Jonathan Berant. Analyzing transformers in embedding space. *arXiv preprint arXiv:2209.02535*, 2022. 2, 6
- [12] Patrick Esser, Sumith Kulal, Andreas Blattmann, Rahim Entezari, Jonas Müller, Harry Saini, Yam Levi, Dominik Lorenz, Axel Sauer, Frederic Boesel, et al. Scaling rectified flow transformers for high-resolution image synthesis. In *ICML*, 2024. 1
- [13] Peng Gao, Le Zhuo, Ziyi Lin, Chris Liu, Junsong Chen, Ruoyi Du, Enze Xie, Xu Luo, Longtian Qiu, Yuhang Zhang, et al. Lumina-t2x: Transforming text into any modality, resolution, and duration via flow-based large diffusion transformers. *arXiv preprint arXiv:2405.05945*, 2024. 2, 5
- [14] Yunhao Ge, Xiaohui Zeng, Jacob Samuel Huffman, Tsung-Yi Lin, Ming-Yu Liu, and Yin Cui. Visual fact checker: enabling high-fidelity detailed caption generation. In *CVPR*, 2024. 3, 1
- [15] Aaron Grattafiori, Abhimanyu Dubey, Abhinav Jauhri, Abhinav Pandey, Abhishek Kadian, Ahmad Al-Dahle, Aiesha Letman, Akhil Mathur, Alan Schelten, Alex Vaughan, et al. The llama 3 herd of models. *arXiv preprint arXiv:2407.21783*, 2024. 2, 4
- [16] Wanggui He, Siming Fu, Mushui Liu, Xierui Wang, Wenyi Xiao, Fangxun Shu, Yi Wang, Lei Zhang, Zhelun Yu, Haoyuan Li, et al. Mars: Mixture of auto-regressive models for fine-grained text-to-image synthesis. *arXiv preprint arXiv:2407.07614*, 2024. 2
- [17] Jack Hessel, Ari Holtzman, Maxwell Forbes, Ronan Le Bras, and Yejin Choi. Clipscore: A reference-free evaluation metric for image captioning. *arXiv preprint arXiv:2104.08718*, 2021. 4
- [18] Martin Heusel, Hubert Ramsauer, Thomas Unterthiner, Bernhard Nessler, and Sepp Hochreiter. Gans trained by a two time-scale update rule converge to a local nash equilibrium. In *NeurIPS*, 2017. 4
- [19] Jonathan Ho and Tim Salimans. Classifier-free diffusion guidance. *arXiv preprint arXiv:2207.12598*, 2022. 5
- [20] Xiwei Hu, Rui Wang, Yixiao Fang, Bin Fu, Pei Cheng, and Gang Yu. Ella: Equip diffusion models with llm for enhanced semantic alignment. *arXiv preprint arXiv:2403.05135*, 2024. 2
- [21] Yushi Hu, Benlin Liu, Jungo Kasai, Yizhong Wang, Mari Ostendorf, Ranjay Krishna, and Noah A Smith. Tifa: Accurate and interpretable text-to-image faithfulness evaluation with question answering. In *ICCV*, 2023. 4
- [22] Kaiyi Huang, Kaiyue Sun, Enze Xie, Zhenguo Li, and Xihui Liu. T2i-compbench: A comprehensive benchmark for open-world compositional text-to-image generation. In *NeurIPS*, 2023. 4
- [23] Aaron Hurst, Adam Lerer, Adam P Goucher, Adam Perelman, Aditya Ramesh, Aidan Clark, AJ Ostrow, Akila Welihinda, Alan Hayes, Alec Radford, et al. Gpt-4o system card. *arXiv preprint arXiv:2410.21276*, 2024. 5, 2
- [24] Ganesh Jawahar, Benoît Sagot, and Djamel Seddah. What does bert learn about the structure of language? In *ACL*, 2019. 2
- [25] Albert Q. Jiang, Alexandre Sablayrolles, Arthur Mensch, Chris Bamford, Devendra Singh Chaplot, Diego de las Casas, Florian Bressand, Gianna Lengyel, Guillaume Lample, Lucile Saulnier, et al. Mistral 7B. *arXiv preprint arXiv:2310.06825*, 2023. 4, 6
- [26] Zhijing Jin, Yuen Chen, Fernando Gonzalez, Jiarui Liu, Jiayi Zhang, Julian Michael, Bernhard Schölkopf, and Mona Diab. Analyzing the role of semantic representations in the era of large language models. *arXiv preprint arXiv:2405.01502*, 2024. 2
- [27] Tero Karras, Miika Aittala, Timo Aila, and Samuli Laine. Elucidating the design space of diffusion-based generative models. In *NeurIPS*, 2022. 1
- [28] Tero Karras, Miika Aittala, Jaakko Lehtinen, Janne Hellsten, Timo Aila, and Samuli Laine. Analyzing and improving the training dynamics of diffusion models. In *CVPR*, 2024. 1

- [29] Chankyu Lee, Rajarshi Roy, Mengyao Xu, Jonathan Raiman, Mohammad Shoeybi, Bryan Catanzaro, and Wei Ping. Nv-embed: Improved techniques for training llms as generalist embedding models. *arXiv preprint arXiv:2405.17428*, 2024. 7
- [30] Baiqi Li, Zhiqiu Lin, Deepak Pathak, Jiayao Li, Yixin Fei, Kewen Wu, Tiffany Ling, Xide Xia, Pengchuan Zhang, Graham Neubig, et al. Genai-bench: Evaluating and improving compositional text-to-visual generation. *arXiv preprint arXiv:2406.13743*, 2024. 2, 4
- [31] Zehan Li, Xin Zhang, Yanzhao Zhang, Dingkun Long, Pengjun Xie, and Meishan Zhang. Towards general text embeddings with multi-stage contrastive learning. *arXiv preprint arXiv:2308.03281*, 2023. 2, 4
- [32] Long Lian, Boyi Li, Adam Yala, and Trevor Darrell. Llm-grounded diffusion: Enhancing prompt understanding of text-to-image diffusion models with large language models. In *TLMR*, 2024. 2
- [33] Shanchuan Lin, Bingchen Liu, Jiashi Li, and Xiao Yang. Common diffusion noise schedules and sample steps are flawed. In *WACV*, 2024. 5
- [34] Zhiqiu Lin, Deepak Pathak, Baiqi Li, Jiayao Li, Xide Xia, Graham Neubig, Pengchuan Zhang, and Deva Ramanan. Evaluating text-to-visual generation with image-to-text generation. In *ECCV*, 2024. 4, 5, 1, 2
- [35] Bingchen Liu, Ehsan Akhgari, Alexander Visheratin, Aleks Kamko, Linmiao Xu, Shivam Shrirao, Chase Lambert, Joao Souza, Suhail Doshi, and Daiqing Li. Playground v3: Improving text-to-image alignment with deep-fusion large language models. *arXiv preprint arXiv:2409.10695*, 2024. 1, 2
- [36] Rosanne Liu, Dan Garrette, Chitwan Saharia, William Chan, Adam Roberts, Sharan Narang, Irina Blok, RJ Mical, Mohammad Norouzi, and Noah Constant. Character-aware models improve visual text rendering. *arXiv preprint arXiv:2212.10562*, 2022. 2
- [37] Zhu Liu, Cunliang Kong, Ying Liu, and Maosong Sun. Fantastic semantics and where to find them: Investigating which layers of generative llms reflect lexical semantics. *arXiv preprint arXiv:2403.01509*, 2024. 2, 6
- [38] Ilya Loshchilov and Frank Hutter. Decoupled weight decay regularization, 2017. 1
- [39] Rui Meng, Ye Liu, Shafiq Rayhan Joty, Caiming Xiong, Yingbo Zhou, and Semih Yavuz. Salesforce AI Research’s SFR-embedding, the top performing text-embedding model. *Salesforce AI Research Blog*, 2024. 4
- [40] Niklas Muennighoff, Nouamane Tazi, Loïc Magne, and Nils Reimers. Mteb: Massive text embedding benchmark. *arXiv preprint arXiv:2210.07316*, 2022. 1, 4
- [41] William Peebles and Saining Xie. Scalable diffusion models with transformers. In *ICCV*, 2023. 1
- [42] Dustin Podell, Zion English, Kyle Lacey, Andreas Blattmann, Tim Dockhorn, Jonas Müller, Joe Penna, and Robin Rombach. Sdxl: Improving latent diffusion models for high-resolution image synthesis. *arXiv preprint arXiv:2307.01952*, 2023. 1, 6, 7
- [43] Alec Radford, Jong Wook Kim, Chris Hallacy, Aditya Ramesh, Gabriel Goh, Sandhini Agarwal, Girish Sastry, Amanda Askell, Pamela Mishkin, Jack Clark, et al. Learning transferable visual models from natural language supervision. In *ICML*, 2021. 1, 2, 3, 5
- [44] Colin Raffel, Noam Shazeer, Adam Roberts, Katherine Lee, Sharan Narang, Michael Matena, Yanqi Zhou, Wei Li, and Peter J Liu. Exploring the limits of transfer learning with a unified text-to-text transformer. *JMLR*, 2020. 1, 2, 3
- [45] Aditya Ramesh, Prafulla Dhariwal, Alex Nichol, Casey Chu, and Mark Chen. Hierarchical text-conditional image generation with clip latents. *arXiv preprint arXiv:2204.06125*, 2022. 1, 2
- [46] Robin Rombach, Andreas Blattmann, Dominik Lorenz, Patrick Esser, and Björn Ommer. High-resolution image synthesis with latent diffusion models. In *CVPR*, 2022. 2, 3, 5, 1
- [47] Olaf Ronneberger, Philipp Fischer, and Thomas Brox. U-net: Convolutional networks for biomedical image segmentation. In *MICCAI*, 2015. 3, 1
- [48] Chitwan Saharia, William Chan, Saurabh Saxena, Lala Li, Jay Whang, Emily L Denton, Kamyar Ghasemipour, Raphael Gontijo Lopes, Burcu Karagol Ayan, Tim Salimans, et al. Photorealistic text-to-image diffusion models with deep language understanding. In *NeurIPS*, 2022. 1, 2, 5, 7
- [49] Christoph Schuhmann, Romain Beaumont, Richard Vencu, Cade Gordon, Ross Wightman, Mehdi Cherti, Theo Coombes, Aarush Katta, Clayton Mullis, Mitchell Wortsman, et al. Laion-5b: An open large-scale dataset for training next generation image-text models. In *NeurIPS*, 2022. 3, 1
- [50] Jacob Mitchell Springer, Suhas Kotha, Daniel Fried, Graham Neubig, and Aditi Raghunathan. Repetition improves language model embeddings. *arXiv preprint arXiv:2402.15449*, 2024. 2, 6, 7
- [51] Gemma Team, Morgane Riviere, Shreya Pathak, Pier Giuseppe Sessa, Cassidy Hardin, Surya Bhupatiraju, Léonard Hussenot, Thomas Mesnard, Bobak Shahriari, Alexandre Ramé, et al. Gemma 2: Improving open language models at a practical size. *arXiv preprint arXiv:2408.00118*, 2024. 1
- [52] Gemma Team, Morgane Riviere, Shreya Pathak, Pier Giuseppe Sessa, Cassidy Hardin, Surya Bhupatiraju, Léonard Hussenot, Thomas Mesnard, Bobak Shahriari, Alexandre Ramé, et al. Gemma 2: Improving open language models at a practical size. *arXiv preprint arXiv:2408.00118*, 2024. 2, 4
- [53] The Mosaic ML Team. Stable diffusion training with mosaicml. *Mosaic Research Blog*, 2023. 1
- [54] Ian Tenney, Patrick Xia, Berlin Chen, Alex Wang, Adam Poliak, R Thomas McCoy, Najoung Kim, Benjamin Van Durme, Samuel R Bowman, Dipanjan Das, et al. What do you learn from context? probing for sentence structure in contextualized word representations. *arXiv preprint arXiv:1905.06316*, 2019. 2
- [55] Tristan Thrush, Ryan Jiang, Max Bartolo, Amanpreet Singh, Adina Williams, Douwe Kiela, and Candace Ross. Winoground: Probing vision and language models for visiolinguistic compositionality. In *CVPR*, 2022. 5
- [56] Hugo Touvron, Thibaut Lavril, Gautier Izacard, Xavier Martinet, Marie-Anne Lachaux, Timothée Lacroix, Baptiste

- Rozière, Naman Goyal, Eric Hambro, Faisal Azhar, et al. Llama: Open and efficient foundation language models. *arXiv preprint arXiv:2302.13971*, 2023. [2](#)
- [57] Patrick von Platen, Suraj Patil, Anton Lozhkov, Pedro Cuenca, Nathan Lambert, Kashif Rasul, Mishig Davaadorj, Dhruv Nair, Sayak Paul, William Berman, Yiyi Xu, Steven Liu, and Thomas Wolf. Diffusers: State-of-the-art diffusion models. *GitHub repository*, 2022. [1](#)
- [58] Liang Wang, Nan Yang, Xiaolong Huang, Binxing Jiao, Linjun Yang, Daxin Jiang, Rangan Majumder, and Furu Wei. Text embeddings by weakly-supervised contrastive pre-training. *arXiv preprint arXiv:2212.03533*, 2022. [2](#)
- [59] Liang Wang, Nan Yang, Xiaolong Huang, Linjun Yang, Rangan Majumder, and Furu Wei. Improving text embeddings with large language models. In *ACL*, 2024. [2](#), [6](#)
- [60] Olivia Wiles, Chuhan Zhang, Isabela Albuquerque, Ivana Kajić, Su Wang, Emanuele Bugliarello, Yasumasa Onoe, Chris Knutsen, Cyrus Rashtchian, Jordi Pont-Tuset, et al. Revisiting text-to-image evaluation with gecko: On metrics, prompts, and human ratings. *arXiv preprint arXiv:2404.16820*, 2024. [4](#)
- [61] Enze Xie, Junsong Chen, Junyu Chen, Han Cai, Yujun Lin, Zhekai Zhang, Muyang Li, Yao Lu, and Song Han. Sana: Efficient high-resolution image synthesis with linear diffusion transformers. *arXiv preprint arXiv:2410.10629*, 2024. [2](#), [5](#)
- [62] Linting Xue, Aditya Barua, Noah Constant, Rami Al-Rfou, Sharan Narang, Mihir Kale, Adam Roberts, and Colin Raffel. ByT5: Towards a token-free future with pre-trained byte-to-byte models. *TACL*, 2022. [2](#)
- [63] An Yang, Baosong Yang, Binyuan Hui, Bo Zheng, Bowen Yu, Chang Zhou, Chengpeng Li, Chengyuan Li, Dayiheng Liu, Fei Huang, et al. Qwen2 technical report. *arXiv preprint arXiv:2407.10671*, 2024. [4](#)
- [64] Michal Yarom, Yonatan Bitton, Soravit Changpinyo, Roei Aharoni, Jonathan Herzig, Oran Lang, Eran Ofek, and Idan Szpektor. What you see is what you read? improving text-image alignment evaluation. In *NeurIPS*, 2023. [4](#)
- [65] Yang Zhang, Yanfei Dong, and Kenji Kawaguchi. Investigating layer importance in large language models. *arXiv preprint arXiv:2409.14381*, 2024. [2](#), [6](#)
- [66] Yanli Zhao, Andrew Gu, Rohan Varma, Liang Luo, Chien-Chin Huang, Min Xu, Less Wright, Hamid Shojanazeri, Myle Ott, Sam Shleifer, et al. Pytorch fsdp: experiences on scaling fully sharded data parallel. *arXiv preprint arXiv:2304.11277*, 2023. [1](#)
- [67] Le Zhuo, Ruoyi Du, Han Xiao, Yangguang Li, Dongyang Liu, Rongjie Huang, Wenze Liu, Lirui Zhao, Fu-Yun Wang, Zhanyu Ma, et al. Lumina-next: Making lumina-t2x stronger and faster with next-dit. *arXiv preprint arXiv:2406.18583*, 2024. [2](#), [5](#)

A Comprehensive Study of Decoder-Only LLMs for Text-to-Image Generation

Supplementary Material

A. Training details

We follow the U-Net [47] based latent diffusion architecture from Stable Diffusion v2 [46] with a [replication training framework](#) by MosaicML [53]. We use Diffusers as our main model codebase for the Variational Autoencoder (VAE), U-Net, and noise scheduler [57]. The configurations all follow the original Stable Diffusion [46]. For each model, we swap the text encoder and freeze all components except for the U-Net. Before the text embeddings are input to the U-Net’s cross-attention blocks, we apply a linear projection from each text encoder’s embedding dimension to 1024 output features for all models. The base U-Net has 865,910,724 trainable parameters, and the additional parameters from the projection for each model are shown in Table A.

For training, we use a 46 million text-image pair subset of the LAION-Aesthetics dataset [49]. We perform center cropping on all training images and LLM-based caption upsampling with VisualFactChecker (VFC) [14]. We train all models for 800,000 iterations at 256×256 resolution with a global batch size of 2,048 on 32 A100 GPUs. We use a caption drop probability of 0.1 and use the AdamW optimizer [38] with a learning rate of 10^{-4} and weight decay of 0.01. We also use additional optimizations such as FlashAttention [10], [half precision GroupNorm](#), [half precision LayerNorm](#), and Fully Sharded Data Parallel’s (FSDP) [66] `SHARD_GRAD_OP` mode for enhanced GPU scaling [53]. Notably, we also pre-compute the VAE image latents and text embeddings for the entire training dataset to reduce repetitive compute time and costs, with each model taking around 7 days to fully train.

B. Prompt upsampling

B.1. Prompting

We use the instruction fine-tuned [Gemma2-9B](#) [51] to perform prompt upsampling at inference. We use the following prompt:

```
You are part of a team that creates images from texts. You work with an assistant that will draw anything you say. For example, outputting "a beautiful morning in the woods with the sun peaking through the trees" will trigger your partner to output an image of a forest morning, as you described.
```

```
You are responsible for helping people create detailed, amazing images. The way to accomplish this is to take their short prompts and make them extremely detailed and descriptive.
```

There are a few rules to follow:

- Try to start with the original input prompt in your output, and then add

details after.

- You will only ever output a single image description per user request.
- Image descriptions must be between 15-80 words. Extra words will be ignored.

With the following generation parameters:

```
do_sample=True
temperature=0.01
top_p=1.0
max_new_tokens=1024
```

B.1.1. Examples

In this subsection, we list a few examples of the upsampled prompts from GenAI-Bench [34] that are used in Figure 4:

A tomato vine with several tomatoes on it, all yellow except the largest which is red \Rightarrow “A tomato vine with several tomatoes on it, all yellow except the largest which is red. The vine is thick and green, with leaves that are a deep, rich green. The tomatoes are plump and juicy, glistening in the sunlight. The largest tomato, a vibrant red, hangs heavy on the vine, contrasting beautifully with the yellow fruit around it.”

A tomato vine with several tomatoes on it, all yellow except the largest which is red \Rightarrow “A larger gorilla hands a smaller mechanical monkey a banana. The gorilla is silverback, with thick fur and a wise expression in its eyes. The mechanical monkey is made of polished brass, with intricate gears visible on its chest and limbs. It has glowing red eyes and a mischievous grin. The banana is ripe and yellow, held out in the gorilla’s massive hand. The background is a lush jungle, with vines and ferns creating a vibrant tapestry.”

C. VQAScore evaluation

C.1. VQAScore details

VQAScore is a metric for evaluating how well a generated image semantically aligns with its text prompt by using visual-question-answering (VQA). It ranges from 0 to 1, where scores closer to 1 represent close alignment with the prompt, and 0 means the generated image doesn’t at all. Intuitively, it measures how well the image understands and represents the prompt, going beyond surface-level similarity. Please refer to the original VQAScore paper [34] for further insight.

C.2. Additional layer-normalized averaging results

We report additional results for our models using layer-normalized average embeddings, which aggregate representations across all layers. Table B presents a comprehensive comparison with the baseline T5 model and models utilizing last-layer embeddings.

C.3. Original CLIP-FlanT5 model

We show results for our models evaluated using the original VQAScore implementation in Tables C, D, E, F, G. As can be

Text Encoders	Embedding Dimension	Extra Parameters
CLIP, T5	1024	1,048,576
Qwen2-1.5B	1536	1,572,864
Gemma2-2B	2304	2,359,296
Qwen2-7B, Gemma2-9B, gte-Gwen2, bge-Gemma2	3584	3,670,016
Mistral-7B, Llama3-8B, sfr-Mistral, Mistral-Instruct	4096	4,194,304

Table A. Additional trainable parameters from adding a linear projection layer from text encoder’s embedding dimensions to 1024 output features before cross-attention.

Model	Embeddings	Avg	Attr.	Scene	Spat.	Action	Part	Count.	Comp.	Differ.	Neg.	Uni.
T5-XXL	last layer	0.741	0.737	0.809	0.741	0.782	0.723	0.677	0.717	0.675	0.599	0.757
T5-XXL	norm avg	0.747	0.748	0.813	0.745	0.780	0.720	0.687	0.736	0.675	0.617	0.760
Qwen2-7B	last layer	0.683	0.679	0.805	0.670	0.724	0.657	0.588	0.603	0.590	0.552	0.763
Qwen2-7B	norm avg	0.740	0.741	0.823	0.740	0.772	0.731	0.680	0.704	0.683	0.589	0.739
Mistral-7B	last layer	0.675	0.667	0.763	0.665	0.711	0.641	0.576	0.556	0.526	0.524	0.726
Mistral-7B	norm avg	0.769	0.774	0.837	0.780	0.802	0.733	0.699	0.716	0.706	0.630	0.789
Llama3-8B	last layer	0.675	0.673	0.767	0.656	0.704	0.667	0.627	0.615	0.568	0.542	0.768
Llama3-8B	norm avg	0.744	0.744	0.831	0.744	0.783	0.705	0.704	0.675	0.659	0.628	0.782
Gemma2-9B	last layer	0.710	0.709	0.794	0.711	0.760	0.705	0.642	0.659	0.617	0.544	0.709
Gemma2-9B	norm avg	0.753	0.757	0.814	0.743	0.790	0.735	0.691	0.703	0.679	0.651	0.770
gte-Qwen2	last layer	0.482	0.486	0.537	0.479	0.497	0.466	0.446	0.393	0.405	0.424	0.437
gte-Qwen2	norm avg	0.654	0.647	0.746	0.626	0.696	0.632	0.539	0.619	0.536	0.538	0.683
sfr-Mistral	last layer	0.710	0.706	0.804	0.707	0.740	0.691	0.661	0.670	0.615	0.608	0.766
sfr-Mistral	norm avg	0.750	0.745	0.839	0.762	0.782	0.713	0.677	0.715	0.706	0.610	0.785
bge-Gemma2	last layer	0.737	0.730	0.824	0.729	0.793	0.722	0.662	0.654	0.641	0.623	0.797
bge-Gemma2	norm avg	0.789	0.787	0.846	0.782	0.821	0.786	0.745	0.776	0.744	0.712	0.810

Table B. VQAScore for models using different embedding strategies: standard last-layer embeddings (last layer) and average embeddings across all normalized layers (norm avg). Highest scores are shown in **bold**. Our results show that using layer-normalized averaging significantly enhances performance and most models outperform T5.

seen in these tables, the [custom CLIP-FlanT5 model](#) introduced in VQAScore paper [34] is not as capable as GPT-4o [23] in discriminating between different models, but still show correlated trends to the GPT-4o results.

C.4. Our GPT-4o implementation

We build upon VQAScore’s support for GPT-4v by replicating the [code](#) and [swapping](#) in the GPT-4o API instead. We also limit the number of tokens returned by setting `top_logprobs = 20`. We found that a simple retry up to 3 times eliminated almost all errors, such as timeout and invalid answer token selections. Apart from enhanced performance, GPT-4o also includes support for prompt caching, allowing for reduced time and costs.

C.5. Random variation

When computing VQAScore with GPT-4o, we generate the 1600 images of upsampled GenAI-Bench prompts for each model. The variation resulting from the choice of random seeds is in the order

of ± 0.004 , depending on the category. The variation from the same seed is ± 0.003 , from non-deterministic CUDA operations and possible non-determinism of the GPT-4o queries.

D. More visual comparisons

We provide additional visual comparisons between the baseline CLIP and T5 models using last-layer embeddings with the Mistral and bge-Gemma2 models using layer-normalized average embeddings. Figure A shows examples from common text-to-image prompts, and Figure B shows additional prompts from GenAI-Bench.

CLIP (*last layer*)T5-XXL (*last layer*)Mistral (*norm avg*)bge-Gemma2 (*norm avg*)

A photo of a Shiba Inu dog with a backpack riding a bike. It is wearing sunglasses and a beach hat.



A high contrast portrait of a very happy fuzzy panda dressed as a chef in a high end kitchen making dough. There is a painting of flowers on the wall behind him.

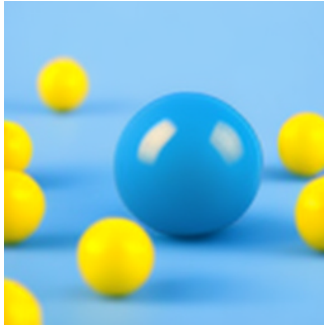


A mischievous ferret with a playful grin squeezes itself into a large glass jar, surrounded by colorful candy. The jar sits on a wooden table in a cozy kitchen, and warm sunlight filters through a nearby window.

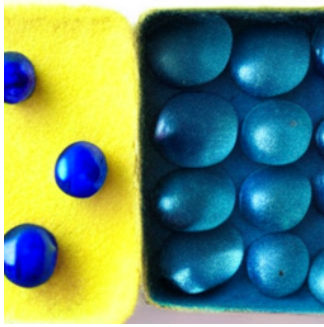
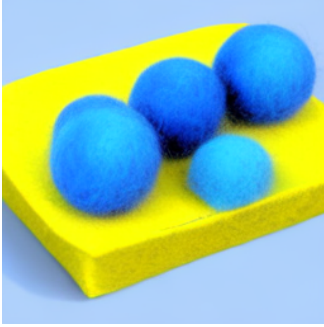


An icy landscape under a starlit sky, where a magnificent frozen waterfall flows over a cliff. In the center of the scene, a fire burns bright, its flames seemingly frozen in place, casting a shimmering glow on the surrounding ice and snow.

Figure A. Visual comparison of images generated with different text encoders. We use last-layer embeddings (*last layer*) from the text encoders of [CLIP-ViT-H/14](#) (354M) and [T5-XXL](#) (4.7B). We also use average layer-normalized embeddings (*norm avg*) from the pre-trained LLM [Mistral-7B](#) (7B) and the fine-tuned embedding model [bge-Gemma2](#) ([bge-multilingual-gemma2](#); 9B).

CLIP (*last layer*)T5-XXL (*last layer*)Mistral (*norm avg*)bge-Gemma2 (*norm avg*)

A scene with two blue balls amidst many yellow ones. The blue balls are slightly larger than the yellow ones and have a smooth, glossy surface that reflects the light.



A yellow felt box has no metallic blue spheres on the left side and has blue metallic spheres on the right side.



There is a large fish aquarium in the center of the luxurious living room, but there are no fish in it. The aquarium is made of polished, rippling glass, reflecting the warm glow of the chandelier above.



A woman with three dogs and no umbrella in the drizzle. Two golden retrievers bound ahead, their tails wagging despite the light rain, while a small terrier trots obediently by her side.

Figure B. Visual comparison of images generated with different text encoders. We use last-layer embeddings (*last layer*) from the text encoders of [CLIP-ViT-H/14](#) (354M) and [T5-XXL](#) (4.7B). We also use average layer-normalized embeddings (*norm avg*) from the pre-trained LLM [Mistral-7B](#) (7B) and the fine-tuned embedding model [bge-Gemma2](#) ([bge-multilingual-gemma2](#); 9B).

Model	Size	Avg	Attr.	Scene	Spat.	Action	Part	Count.	Comp.	Differ.	Neg.	Uni.
CLIP _{ViT-H/14}	354M	0.761	0.762	0.790	0.765	0.762	0.749	0.755	0.758	0.729	0.710	0.771
T5-XXL	4.7B	0.795	0.795	0.816	0.803	0.803	0.780	0.799	0.800	0.793	0.739	0.804
Qwen2-7B	7B	0.772	0.772	0.798	0.777	0.782	0.761	0.760	0.759	0.748	0.712	0.785
Mistral-7B	7B	0.767	0.765	0.787	0.771	0.771	0.751	0.756	0.753	0.733	0.710	0.780
Llama3-8B	8B	0.770	0.769	0.795	0.773	0.775	0.767	0.767	0.768	0.757	0.721	0.793
Gemma2-9B	9B	0.782	0.782	0.801	0.790	0.787	0.776	0.781	0.779	0.769	0.708	0.784
gte-Qwen2	7B	0.597	0.605	0.604	0.609	0.579	0.588	0.602	0.620	0.605	0.605	0.611
sfr-Mistral	7B	0.782	0.780	0.810	0.790	0.782	0.768	0.786	0.786	0.777	0.738	0.794
Mistral-7B _{Instruct}	7B	0.777	0.776	0.799	0.781	0.781	0.765	0.782	0.771	0.758	0.720	0.782
bge-Gemma2	9B	0.786	0.782	0.808	0.790	0.790	0.774	0.786	0.773	0.781	0.750	0.792

Table C. Original VQAScore for models using embeddings extracted from the last layer. We use text encoders from CLIP-ViT-H/14 (354M) and T5-XXL (4.7B), along with four popular open-source pre-trained LLMs: Qwen2 (7B), Mistral-7B (7B), Llama3 (8B), and Gemma2 (9B). Additionally, we include three embedding models fine-tuned on these LLMs: gte-Qwen2 (gte-Qwen2-7B-instruct; 7B), sfr-Mistral (SFR-Embedding-2_R; 7B), and bge-Gemma2 (bge-multilingual-gemma2; 9B). We also include an instruction fine-tuned model, Mistral-7B-Instruct (7B).

Model	Layer	Avg	Attr.	Scene	Spat.	Action	Part	Count.	Comp.	Differ.	Neg.	Uni.
T5-XXL	25 (last)	0.795	0.795	0.816	0.803	0.803	0.780	0.799	0.800	0.793	0.739	0.804
Mistral-7B	33 (last)	0.782	0.780	0.810	0.790	0.782	0.768	0.786	0.786	0.777	0.738	0.794
Mistral-7B	32	0.783	0.782	0.802	0.785	0.790	0.775	0.783	0.766	0.779	0.726	0.786
Mistral-7B	15	0.783	0.785	0.811	0.787	0.788	0.774	0.795	0.783	0.779	0.724	0.783
Mistral-7B	0 (first)	0.660	0.661	0.702	0.657	0.646	0.630	0.655	0.680	0.640	0.605	0.692

Table D. Original VQAScore for models using embeddings extracted from individual layers of Mistral-7B (7B). We include the baseline T5-XXL (4.7B) model using embeddings extracted from the last layer as a reference.

Model	Embeddings	Avg	Attr.	Scene	Spat.	Action	Part	Count.	Comp.	Differ.	Neg.	Uni.
T5-XXL	last layer	0.795	0.795	0.816	0.803	0.803	0.780	0.799	0.800	0.793	0.739	0.804
T5-XXL	norm avg	0.791	0.795	0.810	0.799	0.796	0.771	0.795	0.813	0.783	0.730	0.799
bge-Gemma2	last layer	0.786	0.782	0.808	0.790	0.790	0.774	0.786	0.773	0.781	0.750	0.792
bge-Gemma2	avg	0.809	0.807	0.822	0.815	0.814	0.793	0.811	0.813	0.794	0.755	0.807
bge-Gemma2	norm avg	0.801	0.801	0.821	0.806	0.806	0.790	0.803	0.805	0.789	0.758	0.813
Mistral-7B	last layer	0.782	0.780	0.810	0.790	0.782	0.768	0.786	0.786	0.777	0.738	0.794
Mistral-7B	avg	0.786	0.785	0.809	0.797	0.793	0.774	0.783	0.780	0.761	0.726	0.788
Mistral-7B	norm avg	0.799	0.798	0.820	0.808	0.810	0.789	0.791	0.796	0.790	0.734	0.805

Table E. Original VQAScore for models using different embedding strategies: standard last-layer embeddings (*last layer*), average embeddings across all layers (*avg*), and average embeddings across all normalized layers (*norm avg*). We evaluate the encoder from T5-XXL (4.7B), the pre-trained LLM Mistral-7B (7B), and the fine-tuned embedding model bge-Gemma2 (bge-multilingual-gemma2; 9B).

Model	Avg	Attr.	Scene	Spat.	Action	Part	Count.	Comp.	Differ.	Neg.	Uni.
bge-Gemma2	0.786	0.782	0.808	0.790	0.790	0.774	0.786	0.773	0.781	0.750	0.792
bge-Gemma2 _{pooled}	0.802	0.801	0.828	0.807	0.806	0.789	0.812	0.806	0.799	0.763	0.835
sfr-Mistral	0.782	0.780	0.810	0.790	0.782	0.768	0.786	0.786	0.777	0.738	0.794
sfr-Mistral _{pooled}	0.782	0.778	0.810	0.779	0.788	0.774	0.778	0.772	0.772	0.739	0.796

Table F. Original VQAScore for models using embeddings extracted from the last layer compared to models with additional conditioning on global pooled embeddings [42]. We evaluate the fine-tuned embedding models bge ([bge-multilingual-gemma2](#); 9B) and sfr ([SFR-Embedding-2_R](#); 7B).

Model	Size	Avg	Attr.	Scene	Spat.	Action	Part	Count.	Comp.	Differ.	Neg.	Uni.
Qwen2	1.5B	0.758	0.759	0.784	0.761	0.760	0.738	0.756	0.753	0.747	0.704	0.755
Qwen2	7B	0.772	0.772	0.798	0.777	0.782	0.761	0.760	0.759	0.748	0.712	0.785
Gemma2	2B	0.770	0.773	0.797	0.774	0.774	0.759	0.783	0.764	0.756	0.710	0.787
Gemma2	9B	0.782	0.782	0.801	0.790	0.787	0.776	0.781	0.779	0.769	0.708	0.784

Table G. Original VQAScore for models with different LLM sizes, using embeddings extracted from the last layer. We evaluate the pre-trained LLMs: [Qwen2](#) (1.5B), [Qwen2](#) (7B), [Gemma2](#) (2B), [Gemma2](#) (9B).